# Lattice and spin excitations of $YFeO_3$: A Raman and density functional theory study

Yu. S. Ponosov and D. Y. Novoselov
*M.N. Mikheev Institute of Metal Physics UB RAS, 620137, S. Kovalevskaya str. 18, Ekaterinburg, Russia and Ural Federal University, Mira St. 19, 620002 Ekaterinburg, Russia*

(Received 5 May 2020; revised 29 June 2020; accepted 28 July 2020; published 12 August 2020)

We report a Raman scattering study of $YFeO_3$ orthoferrite. Polarized Raman measurements in wide temperature range and first-principles calculations provided the assignment of the observed phonon modes to vibrational symmetries and atomic displacements. We did not observe previously reported anomalies in the behavior of phonon frequencies near the temperature of the antiferromagnetic transition. Temperature behavior of frequencies and linewidths of most phonons may be described by known expressions for cubic and quartic anharmonicity, which implies a significant contribution of phonon-phonon interaction. At the same time, several phonons exhibit asymmetric profiles and anomalies in the behavior of their widths, which indicates an interaction with a continuum of some excitations. The most striking evidence of this is the observation of the coupling of the $B_{2g}$ phonon at 640 $cm^{-1}$ with the two-magnon continuum, expressed in anomalous phonon self-energies in the vicinity of $T_N$. The appearance of a broad continuum of low-frequency excitations when approaching $T_N$, which is possibly induced by the damping of spin excitations due to interaction with the lattice, has been revealed. This interaction can lead to additional contributions to the renormalization of phonon self-energies, formally described by formulas for anharmonic effects. Phonon scattering induced by defects has been identified. The temperature behavior of resonant second-order phonon and two-magnon scattering was studied in detail.

DOI: 10.1103/PhysRevB.102.054418

## I. INTRODUCTION

The rare-earth orthoferrites, $RFeO_3$ perovskites, have attracted considerable interest due to their rich variety of magnetic properties [1–3]. At ambient conditions they have an orthorhombic *Pnma* structure (space group 62, $D_{2h}^{16}$). All members of the family possess a canted antiferromagnetic structure arising from spin moments of the $Fe^{3+}$ cations. The antiferromagnetic ordering of the iron ions occurs at a Neel temperature $T_N$ around 640 to 740 K.

In the $YFeO_3$ system having one magnetic subsystem, superexchange magnetic interaction occurs between two $Fe^{3+}$ ions, which are separated by an $O^{2-}$ ion. Below the Neel temperature $T_N \sim 640$ K, the Fe spins order antiferromagnetically with an easy axis along the *a* direction of the crystal, with a small canting ($\sim 0.5^\circ$) along the orthorhombic *b* direction. Weak ferromagnetism along the *c* direction of the crystal is caused by two mechanisms: antisymmetric exchange or Dzyaloshinsky-Moriya (DM) interaction and single-ion magnetocrystalline anisotropy.

Recent results suggest the existence of multiferroic properties in polycrystalline $YFeO_3$ [4,5]. Work [4] presented direct experimental evidence for the simultaneous coexistence of ferroelectricity and weak ferromagnetism in $YFeO_3$ at room temperature. As proposed previously for isostructural compounds $SeCuO_3$ and $TeCuO_3$ [6], a dielectric anomaly in a magnetodielectric material can arise due to the spin-phonon coupling. The paper [5] investigated the reasons for the anomalous behavior of the dielectric constant found in the vicinity of $T_N$ for $YFeO_3$ polycrystalline samples. Their studies on the pure $YFeO_3$ polycrystalline samples discovered significant coupling between the spin and lattice degrees of freedom at and below $T_N$ which correlated to find dielectric anomalies both in the low temperature and also in the vicinity of $T_N$. This conclusion is based, in particular, on the observation of very significant anomalies in the self-energies of a number of phonon lines in $YFeO_3$ Raman spectra near $T_N$.

Numerous studies of the Raman spectra of rare-earth orthoferrites have been published [2,5,7–15]. Inelastic scattering of light by phonons and single- and two-magnon excitations was studied on single-crystal samples [2,7,8,10,11]. First-principles calculations of the phonon spectra of rare-earth orthoferrites were performed for comparison with experiment [11,13–15]. Surprisingly, we did not find a systematic Raman study of the phonon spectrum of $YFeO_3$ performed on single crystals. The single-crystalline spectra published in [16,17] are uninformative even in comparison with Raman studies on polycrystals.

Therefore, one of the goals of this work was to study the polarized Raman spectra of $YFeO_3$ and to compare the data obtained with the first-principles calculation of the phonon spectrum. Although the temperature behavior of single-magnon excitations is well studied, the temperature dependencies of the phonon frequencies and linewidths have not been studied on single crystals. Therefore, we further investigated this behavior with an emphasis on the $T_N$ neighborhood to compare single-crystalline data with the anomalous behavior of self-energy for a number of phonons reported in [5] after measurements on polycrystalline samples. Besides, we first traced the temperature evolution of the two-magnon light scattering spectrum, which was previously observed in $YFeO_3$ at 80 K [8].

 

TABLE I. Calculated by DFT + $U$ and DFT + $U$ + SO as well as experimental [9] structural data in reduced coordinates of the orthoferrite $YFeO_3$ with *Pnma* space-group symmetry.

| | | | DFT + $U$ | | | DFT + $U$ + SO | | | Expt. [9] | | |
|---|---|---|---|---|---|---|---|---|---|---|---|
| | | | $a$ 5.5743 | $b$ 7.6096 | $c$ 5.2654 | $a$ 5.5715 | $b$ 7.6079 | $c$ 5.2629 | $a$ 5.5916 | $b$ 7.6032 | $c$ 5.2803 |
| Atom | Site | Wyckoff pos. | $x$ | $y$ | $z$ | $x$ | $y$ | $z$ | $x$ | $y$ | $z$ |
| Y | Y1 | 4$c$ | 0.0685 | 0.2500 | −0.0190 | 0.0685 | 0.2500 | −0.0190 | 0.0688 | 0.2500 | −0.0179 |
| Fe | Fe1 | 4$b$ | 0.0000 | 0.0000 | 0.5000 | 0.0000 | 0.0000 | 0.5000 | 0.0000 | 0.0000 | 0.5000 |
| O | O1 | 4$c$ | 0.4588 | 0.2500 | 0.1151 | 0.4587 | 0.2500 | 0.1151 | 0.4600 | 0.2500 | 0.1105 |
| O | O2 | 8$d$ | −0.3033 | −0.0583 | 0.3068 | −0.3033 | −0.0583 | 0.3069 | −0.3045 | −0.0575 | 0.3075 |

## II. EXPERIMENTAL AND CALCULATION DETAILS

Single crystals of $YFeO_3$ were grown by a floating zone method associated with an image furnace of URN2-ZM type operated in a different atmosphere in the Moscow Power Engineering Institute by modified Czochralski method with radiation and combined with HF heating [18]. Two single crystals Nos. 1 and 2 used for measurements were not certified for chemical composition. Samples were oriented and cut along the crystallographic planes with ∼3 mm ×3 mm dimensions. Polarized Raman measurements in the temperature range of 300 to 850 K were performed in backscattering geometry from the cleaved chips of these planes using RM1000 Renishaw microspectrometer equipped with 532-nm solid-state laser and 633 helium-neon laser. Respective Linkam stage was used for temperature variation. Very low power (up to 1 mW) was used to avoid local heating of the sample. A pair of notch filters with a cutoff at 60 $cm^{-1}$ was used to reject light from the 633-nm laser line. To get as close to the zero frequency as possible, with 532-nm excitation we used a set of three volume Bragg gratings (VBG) to analyze the scattered light. This made it possible to reach frequencies of 10 $cm^{-1}$ and to get access to the anti-Stokes spectrum. The resolution of our Raman spectrometer is estimated to be 2–3 $cm^{-1}$.

The first-principles calculations were performed in the framework of the density functional theory (DFT) using the projector-augmented wave (PAW) method [19] implemented in the Vienna *ab initio* simulation package (VASP) [20] with the exchange-correlation energy described by the generalized gradient approximation (GGA) using the Perdew-Burke-Ernzerhof (PBE) functional [21]. The strong electronic correlations on the $d$ states of Fe ions were taken into account using the DFT + $U$ method [22] with effective Hubbard correction parameter $U_{\text{eff}} = 4$ eV [23]. We also performed calculations taking into account a spin-orbit coupling within the DFT + $U$ +SO method. We used the Monkhorst-Pack $k$-point mesh 6 × 4 × 6 division. The volume and the shape of the unit cell, as well as the ionic coordinates, were fully relaxed. To obtain the phonon dispersion, the following phonon calculations were performed by the frozen-phonon method within the PHONOPY package [24]. For the force constants calculations, the 2 × 1 × 2 supercell was applied.

$YFeO_3$ is a multiferroic system and it has weak ferromagnetism due to a small canting of the large moments ordered antiferromagnetically. The reason for the existence of the canting is the presence of a spin-orbit coupling [23]. We have performed full structural optimization using DFT + $U$ and DFT + $U$ + SO starting from the experimental lattice parameters [9]. The obtained lattice constants and atomic positions shown in Table I are close to the experimental values [9]. By comparing the results obtained with both methods we conclude that the differences between the structural parameters are extremely small, which suggests that the spin-orbit interaction does not significantly affect the lattice dynamics. The reason is the extremely small canting angle of the antiferromagnetic structure as was shown early in the work [23]. In this regard, we performed further calculations of the phonon spectra by the DFT + $U$ method. The most stable [23] AFM-G type magnetic configuration, specified as the starting one, has been survived during full structural optimization. The magnitude of the magnetic moment per iron atom was 4.17 $\mu_B$ which is in good agreement with published data [23].

## III. RESULTS AND DISCUSSION

### A. First-order phonon Raman spectra of $YFeO_3$

First of all, we present the results of group-theoretical analysis of vibrational spectra of $YFeO_3$ to determine the number and symmetry of modes, which are expected to contribute to Raman scattering spectra. $YFeO_3$ structure is characterized by *Pnma* space group and there are 20 atoms in the unit cell. The following optical modes should be presented in the Γ point in this structure:

$$\Gamma = 7A_g + 5B_{1g} + 7B_{2g} + 5B_{3g} + 9B_{1u} + 7B_{2u} + 9B_{3u} + 8A_u, \quad (1)$$

24 of them are Raman active. The phonon spectrum calculated using a finite displacement method is shown in Fig. 1. It can be seen from Fig. 1 that there are no imaginary phonon modes, which indicates its dynamic stability. The low-frequency branches of the phonon spectra are the acoustic phonon modes below 5 THz (170 $cm^{-1}$) which mainly contributed by heavy Y atoms with slight contributions from Fe and O. The middle frequency range from 5 (170) to 12 (400) THz ($cm^{-1}$) is formed by the optical branches with a mixed character of Fe-O modes. The optical modes of the high-frequency range are predominantly formed due to vibrations of oxygen atoms since they are the lightest in this compound.

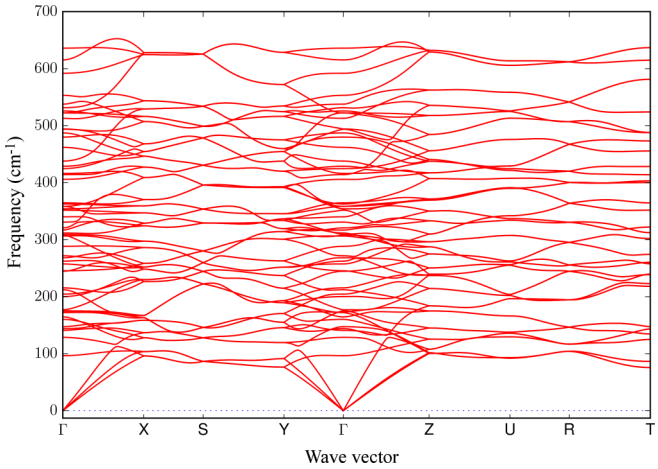


FIG. 1. Calculated phonon dispersion of $YFeO_3$.

Figure 2 shows polarized Raman spectra $YFeO_3$ measured at $T = 300$ K on different planes of a single crystal No. 1. In spectra, we observed all the expected 24 modes. As can be seen from Fig. 2, some vibrations of $B$ symmetries have very low intensities. Also, sometimes they have frequencies close to intense vibrations of $A_g$ symmetry, which makes it difficult to observe them. Thus, almost identical frequencies were found for the vibrations of $A_g$, $B_{1g}$, and $B_{3g}$ symmetries near 428 $cm^{-1}$, as well as for the vibrations of $A_g$ and $B_{2g}$ symmetries near 498 $cm^{-1}$. Bearing in mind such close proximity of vibration frequencies of various symmetries, we believe that a correct analysis of the phonon spectrum is possible only when using polarization measurements on single crystals. The measurements performed on polycrystals [5,9,12,15], as a rule, find a number of the most intense $A_g$ and $B_{2g}$ lines and cannot resolve closely located lines of other symmetries. Attempts to decompose unpolarized spectra into overlapping lines, obviously, cannot give reliable results regarding the temperature behavior of the phonon spectrum. The frequencies of the observed in $YFeO_3$ phonon lines are presented in Table II together with the data obtained by the frozen-phonon calculations. The performed calculation shows a good agreement with the experimental frequencies.

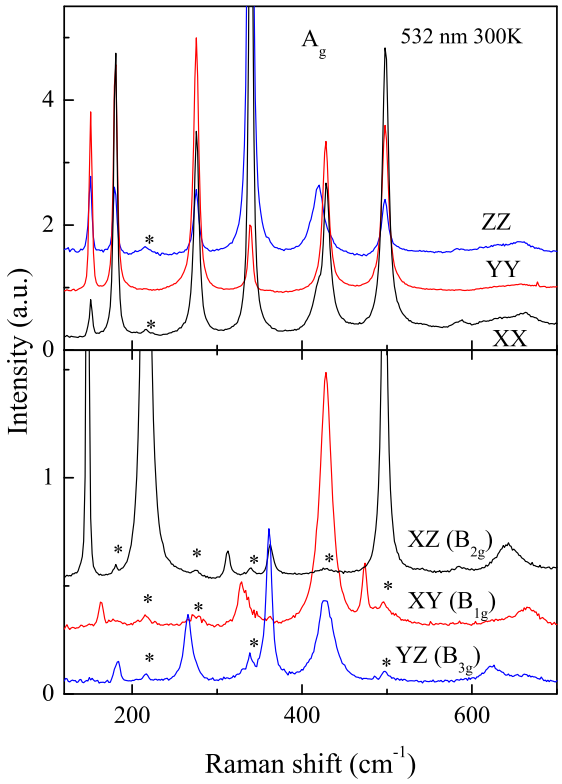


FIG. 2. Raman spectra of $YFeO_3$, measured in different polarization geometries with 532-nm excitation at 300 K. The peaks marked by asterisks are polarization leakages of strong $A_g$ and $B_{2g}$ lines.

Numerous Raman studies of rare-earth orthoferrites [5,9–15] reported observation of rather intense lines at ∼630 $cm^{-1}$. They are observed mainly in polarized geometry, which indicates its $A_g$ symmetry. However, as shown in the previous *ab initio* calculation for $SmFeO_3$ [11], and in our calculation for $YFeO_3$, only $B$ modes should be presented in this region of the spectrum. The authors of previous Raman studies suggested that the appearance of this line is caused either by a violation of the selection rules for the wave vector due to the presence of defects in the sample or by second-order Raman scattering. Raman spectra of two investigated $YFeO_3$ crystals are presented in Fig. 3. As can be seen, the frequencies and widths of the phonon lines of the two samples practically coincide, however, the strong 630-$cm^{-1}$ line is observed in sample No. 2 (in XZ, $B_{2g}$ geometry with much less intensity) and is absent in the spectrum of sample No. 1. This convincingly confirms the hypothesis of the defective origin of this line which will be discussed further in Sec. III C. The absence of a broadening of phonon lines may be due to the presence of defects in the iron sublattice, whose vibrations are inactive in the Raman spectrum. The absence of 630-$cm^{-1}$ line in the spectrum of sample No. 1 makes it possible to observe weak $B_{2g}$ and $B_{3g}$ lines in this spectral region. Nevertheless, it can be seen that weak extra lines, possibly of a defective nature, are also observed at other frequencies of the spectra near 580 $cm^{-1}$.

The total and partial densities of phonon states obtained within DFT + $U$ for $YFeO_3$ is shown in Fig. 4. As can be seen, the peak frequency at 630 $cm^{-1}$ coincides with the frequency of the high-frequency narrow peak in the density of phonon states. This also suggests its connection with defect-induced Raman scattering reflecting the density of phonon states.

In order to study the proposed effects of spin-phonon interaction in $YFeO_3$ [5] in details, the Raman spectra were measured between 300 and 850 K. The frequencies and linewidths of most phonon lines were obtained by peak fitting to a Voigt function, which is a Lorentzian folded with a Gaussian that accounts for the spectrometer bandwidth. With increasing temperature, the frequencies of almost all lines in the spectra decrease, and their widths increase (Fig. 5). Such behavior may come from anharmonic effects. An account of the cubic and quartic anharmonicities leads to well-known expressions

TABLE II. Calculated and experimentally found at 300-K frequencies (in $cm^{-1}$) of Raman active modes for $YFeO_3$ with respect to the polarization geometry in which they are observed. Corresponding irreducible representations are also shown.

| | | Frequency ($cm^{-1}$) | | | | | | |
|---|---|---|---|---|---|---|---|---|
| | | | Experiment | | | | | |
| No. | Symmetry | Theory | XX $A_g$ | YY $A_g$ | ZZ $A_g$ | XY $B_{1g}$ | XZ $B_{2g}$ | YZ $B_{3g}$ |
| 1 | $A_g$ | 147 | 151 | 151 | 151 | | | |
| 2 | $A_g$ | 175 | 180.5 | 180.5 | | | | |
| 3 | $A_g$ | 272 | 276 | 276 | 276 | | | |
| 4 | $A_g$ | 330 | 340 | 340 | 340 | | | |
| 5 | $A_g$ | 414 | 419 | 419 | | | | |
| 6 | $A_g$ | 428 | 428 | 428 | 428 | | | |
| 7 | $A_g$ | 493 | 498 | 498 | 498 | | | |
| 8 | $B_1g$ | 173 | | | | 163.5 | | |
| 9 | $B_1g$ | 258 | | | | 328.5 | | |
| 10 | $B_1g$ | 354 | | | | 428 | | |
| 11 | $B_1g$ | 424 | | | | 474 | | |
| 12 | $B_1g$ | 592 | | | | 660 | | |
| 13 | $B_2g$ | 144 | | | | | 147.5 | |
| 14 | $B_2g$ | 212 | | | | | 216.5 | |
| 15 | $B_2g$ | 309 | | | | | 312.5 | |
| 16 | $B_2g$ | 359 | | | | | 363 | |
| 17 | $B_2g$ | 487 | | | | | 497 | |
| 18 | $B_2g$ | 537 | | | | | 532 | |
| 19 | $B_2g$ | 615 | | | | | 641 | |
| 20 | $B_3g$ | 160 | | | | | | 184 |
| 21 | $B_3g$ | 315 | | | | | | 266 |
| 22 | $B_3g$ | 416 | | | | | | 361 |
| 23 | $B_3g$ | 462 | | | | | | 428 |
| 24 | $B_3g$ | 636 | | | | | | 624 |

for the phonon frequency shift and linewidth [25,26]:

$$\Delta\omega_{an}(T) = \Delta\omega_{\text{therm}} + A[1 + 2n(\omega/2)] + B[1 + 3n(\omega/3) + 3n^2(\omega/3)], \quad (2)$$

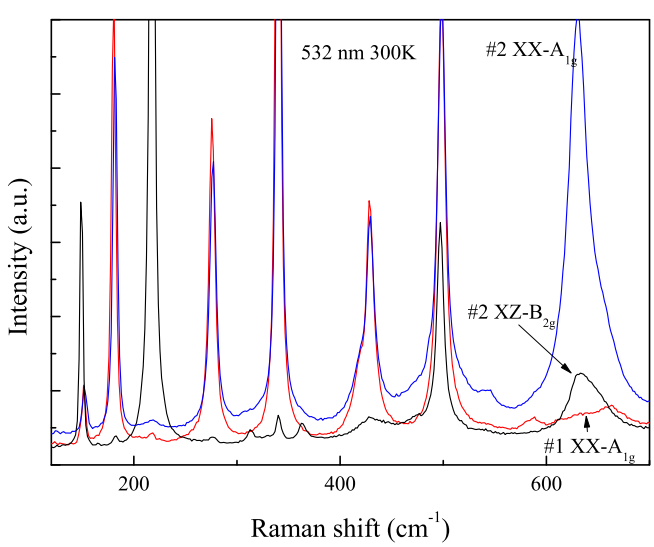


FIG. 3. Raman spectra measured from $YFeO_3$ crystals Nos. 1 and 2 in XX polarization geometry at 300 K. XZ spectrum of crystal No. 2 is also shown.

$$\Gamma(T) = \Gamma_0 + C[1 + 2n(\omega/2)] + D[1 + 3n(\omega/3) + 3n^2(\omega/3)], \quad (3)$$

$$\Delta\omega_{\text{therm}} = \omega_0\left[\exp\left(-\gamma\int_0^T \alpha(T')dT'\right) - 1\right]. \quad (4)$$

The bare linewidth $\Gamma_0$ includes contributions from different defects, $A$ and $B$ are fitting parameters related to the

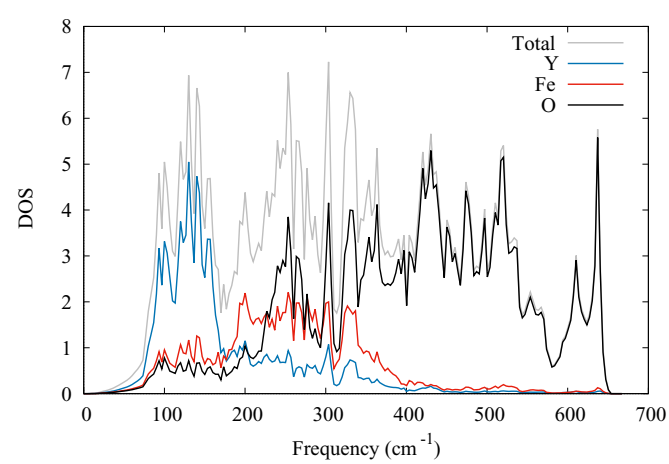


FIG. 4. Calculated total and partial densities of states of $YFeO_3$.

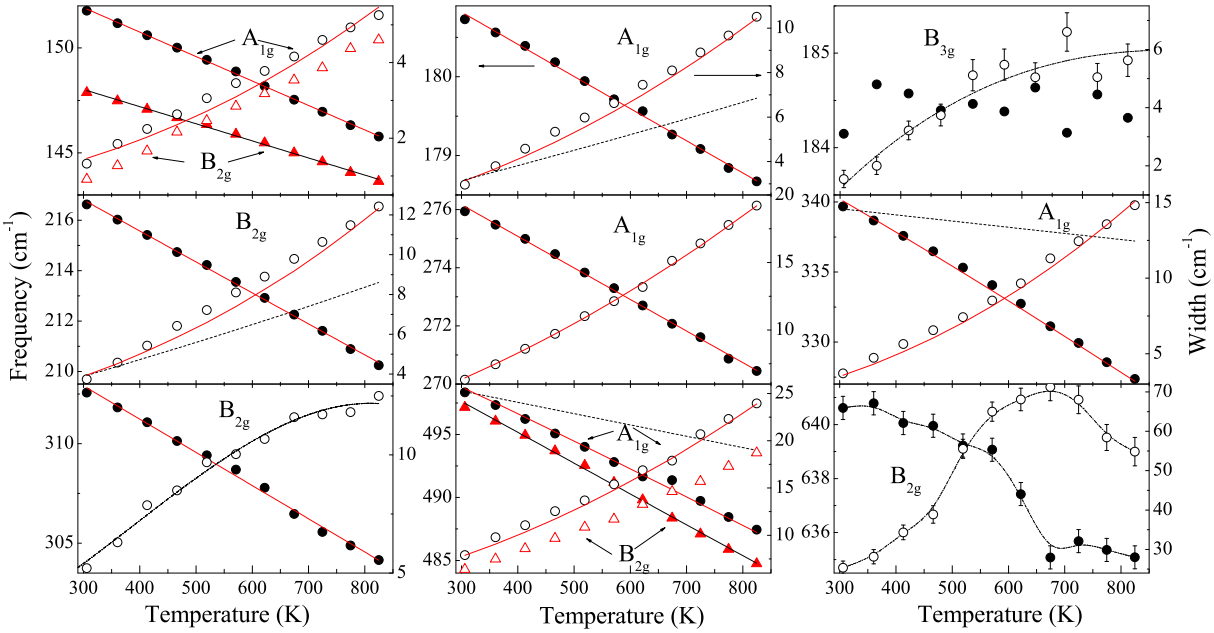


FIG. 5. Temperature dependencies of the frequency (filled circles) and full width at half-maximum (empty circles) of the number $A_g$ and $B_{2g}$ modes. Solid lines are linear fits of frequency and fits of linewidth by expressions and (3). Dashed lines show anharmonic width dependence using cubic term only (phonons 180 and 216 cm$^{-1}$) and thermal expansion contribution to phonon frequency (340 and 498 cm$^{-1}$). Dotted-dashed lines are the guide to the eye.

third-order coefficients in the expansion of the lattice potential in normal coordinates, $C$ and $D$ are fitting parameters related to the fourth-order coefficients, $n$ is Bose-Einstein factor.

For most phonons, smooth dependencies of frequencies and linewidths are observed in the entire studied temperature range. So, we did not observe the reported in [5] anomalies in the temperature dependencies of frequencies for sufficiently localized phonons at 150, 180, 340, and 498 cm$^{-1}$. Unfortunately, the data on thermal expansion coefficient $\alpha(T)$ are known only for the $a$ direction of the $YFeO_3$ crystal [27]. Since both the frequencies of the phonon spectrum and the expansion for this axis are close in the case of the structural analog of $YCrO_3$ [28,29], we used the available data for $YCrO_3$ and the calculated bulk modulus [30] to estimate the contribution of thermal expansion to the frequency shift. Estimates of this contribution and the total contribution (thermal expansion + cubic anharmonicity) are shown for two $A_g$ phonons at 340 and 498 cm$^{-1}$ in Fig. 5. The obtained dependencies are almost linear and describe experimental ones well. For other phonons in Fig. 5, the frequency behavior is also well described by a linear dependence, which implies the sufficiency of cubic anharmonicity combined with the contribution of thermal expansion to fit the phonon energies. Nevertheless, the correct description of the behavior of phonon energies in $YFeO_3$ requires knowledge of both thermal expansion and the effect of pressure on the phonon spectrum.

In contrast to frequency behavior, the behavior of the linewidth cannot be described by only one cubic term, shown for the phonon at 180 and 216 cm$^{-1}$. A quartic anharmonicity [third term in (3)] addition is necessary to describe the temperature dependence of the linewidths of most phonons. However, it is interesting that clear Fano interference profiles were observed for $A_g$ lines at 275 and 498 cm$^{-1}$ (Fig. 6). In this case, the phonon line shape should be described by the asymmetric Breit-Wigner-Fano (BWF) profile expression [31]

$$I(\omega) = \pi\rho(\omega)T_e^2\frac{(q+\epsilon)^2}{1+\epsilon^2}, \tag{5}$$

$$\epsilon = \frac{\omega-\omega_0-V^2R(\omega)}{\Gamma}, \tag{6}$$

$$q = \frac{V[T_p/T_e+V^2R(\omega)]}{\pi V^2\rho(\omega)}, \tag{7}$$

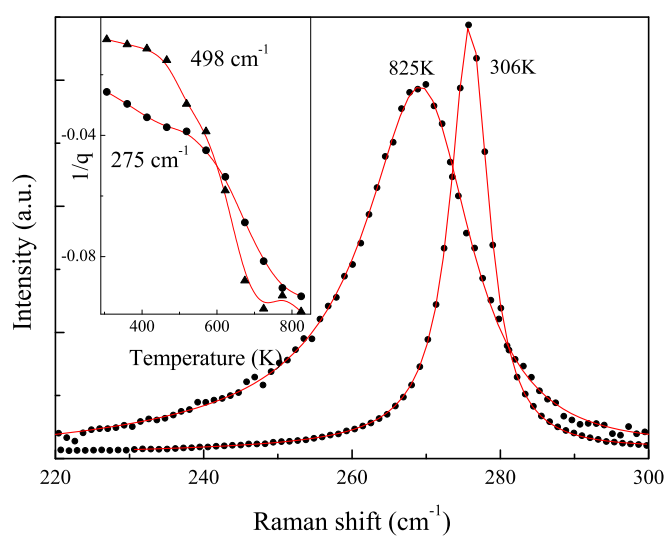


FIG. 6. Line shapes of $A_g$ phonon near 275 cm$^{-1}$ fitted by expression (5) at two temperatures. Inset shows temperature dependence asymmetry parameter $1/q$.

where $\omega_0$ and $R(\omega)$ are a bare (uncoupled) mode frequency and the Hilbert transform of continuum density of states $\rho(\omega)$. $T_e$ and $T_p$ are scattering amplitudes for continuum and phonon. Continuum-phonon interaction with matrix element $V$ determines the phonon width $\Gamma = 2[\Gamma_0 + \pi V^2 \rho(\omega)]$ ($\Gamma_0$ is the phonon width in absence of interaction). This interaction also shifts the phonon energy to $\omega = \omega_0 + V^2 R(\omega)$. Observed 275- and 498-cm$^{-1}$ line profiles clearly indicate the interaction of both phonons with a certain continuum of excitations, which can lead to additional contributions to the phonon self-energies, in addition to anharmonic ones. As one can see, the asymmetry parameter $1/q$ decreases up to $T_N$ and then saturation occurs for both $A_g$ lines (Fig. 6). However, the temperature behavior of width of both lines is well described by formula (3) (Fig. 5). Unfortunately, the sums over wave vectors of the three phonons involved in the quartic anharmonicity process are mathematically intractable, and the expressions given in [26] are difficult to evaluate explicitly. Asymmetric line profiles were also observed for modes at 312 and 640 cm$^{-1}$.

A number of phonons of $B$ symmetries show a more complex temperature behavior of their widths (Fig. 5). Due to the low intensity of these lines and the overlap with other lines of the spectrum, their frequencies and widths are extracted with large errors. However, Fig. 5 shows that the linewidths of phonons at 184, 312, and 640 cm$^{-1}$ demonstrate a saturation tendency and even peak structure at temperatures at $T \geqslant T_N$. Small humps are visible in the dependencies of the linewidth near 600 K for phonons at 147, 151, 181, and 216 cm$^{-1}$ associated with Y atom motions. Interestingly, the $B_{3g}$ mode at 184 cm$^{-1}$ does not change its energy in the studied temperature range. Taking into account the small but negative contribution of thermal expansion, the frequency of this mode increases anomalously with increasing temperature, which raises the question of the nature of the broadening of this line. The out-of-phase motion of Y atom in $x$-$z$ and $y$ directions and similar displacements of O(2) atoms are characteristic for this vibration. The $B_{2g}$ vibration at 312 cm$^{-1}$ produces the strong bending of the Fe-O(2) planes in the $a$ direction, while the $B_{2g}$ phonon at 640 cm$^{-1}$ produces stretching of Fe-O(2) bonds in these planes. Such distortions should substantially modulate the exchange interaction and can determine strong spin-phonon coupling, as will be shown below.

### B. Two-magnon and spin-induced Raman scattering in $YFeO_3$

Koshizuka [8] suggested that the broad peak observed in $YFeO_3$ spectrum near 970 cm$^{-1}$ at 80 K is due to two-magnon scattering, when excitations of magnon pairs with $q$ and $-q$ contribute to the spectrum. This peak has a significant intensity with parallel polarizations of the incident and scattered light YY and cross polarizations XZ and at room temperature it has a maximum near 920 cm$^{-1}$ (Fig. 9). Such a peak should reflect the density of magnon states with the dominant contribution of short-wave magnons and provides information on the exchange interaction. Since the zone-boundary magnons are located near 65 meV (525 cm$^{-1}$) [32,33], a doubled value gives the estimated frequency of two-magnon scattering of 1050 cm$^{-1}$. Magnon interactions may be the reason that the observed peak energy of 970 cm$^{-1}$ is slightly lower.

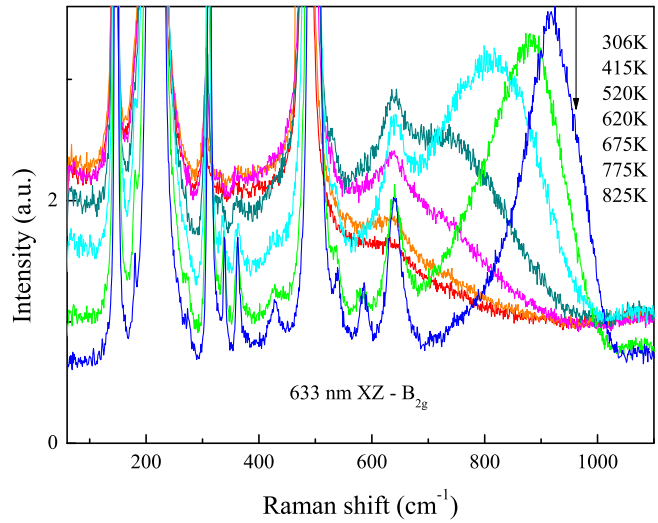


FIG. 7. Temperature evolution of two-magnon spectra of $YFeO_3$ crystal. Excitation wavelength 633 nm.

We studied the previously unexplored temperature behavior of two-magnon scattering in $YFeO_3$. Figure 7 demonstrates the broadening and softening of the two-magnon peak to 700 cm$^{-1}$ at a temperature of 650 K, after which its intensity is almost unobservable. The temperature dependence of the peak intensity is shown in Fig. 8 together with the spectra of two single-magnon modes at 11 and 18 cm$^{-1}$ in the crystal under study. The temperature dependence of their frequencies is similar to that measured in [8]. It should be noted that the intensity of the two-magnon peak tends to zero at $T \geqslant T_N$, although in other antiferromagnets it has a noticeable value in the paramagnetic phase. The same evolution of both the two-magnon peak and the broad low-frequency continuum is observed for the polarized YY geometry ($B_{2g}$). The disappearance of the two-magnon peak is accompanied by the growth of the continuum of excitations in the low-frequency region of the spectrum, and this growth continues to the temperature $\sim T_N$ and then ceases. A similar situation was previously observed in the parent antiferromagnetic compositions of high-temperature superconductors. The two-magnon peak at 2600 cm$^{-1}$ in RBaCuO substantially decreased in intensity, softened and broadened, and a broad background appeared in the low-frequency region of the spectrum [34,35]. One explanation for this behavior involves the damping of magnetic excitations due to the strong spin-lattice interaction. In this case, it is logical to assume that this interaction can contribute to the phonon self-energies since in $YFeO_3$ the phonon and magnon frequencies overlap. This is confirmed by the behavior of the self-energy of $B_{2g}$ phonon at 640 cm$^{-1}$. With increasing temperature, the two-magnon continuum of the same symmetry passes through this phonon, which leads to an increase in its damping and a softening of the frequency. A similar effect of the coupling of the phonon and two-magnon excitations was previously observed in $Cd_2Os_2O_7$ [36].

In the spin systems, quasielastic scattering has been frequently reported in Raman scattering measurements [37]. Usually, its origin is explained in terms of spin-energy

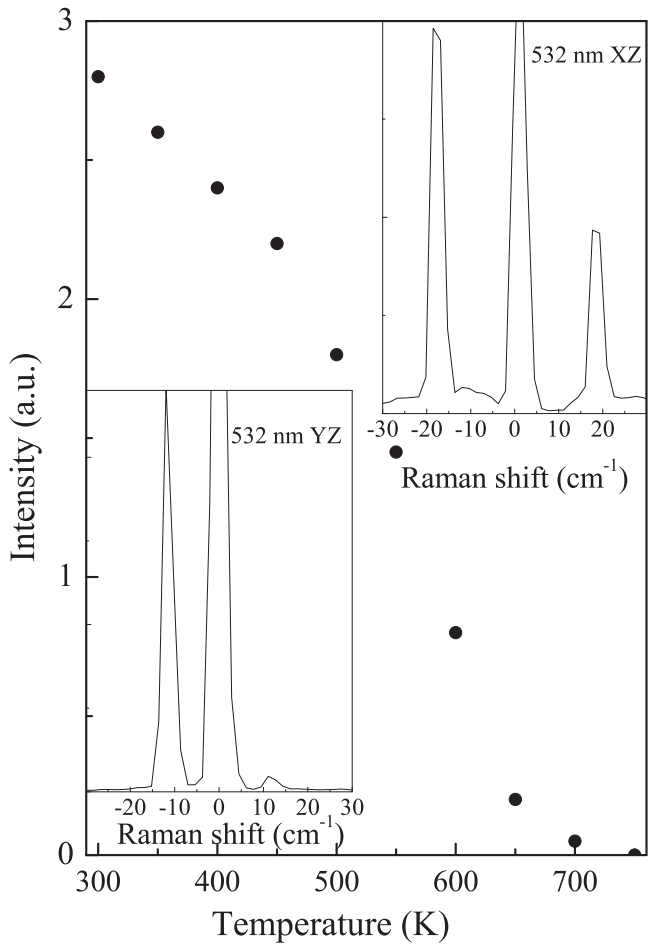


FIG. 8. Temperature dependence of two-magnon peak intensity. Insets show Raman spectra of two $q = 0$ one-magnon modes of $YFeO_3$ crystal at room temperature.

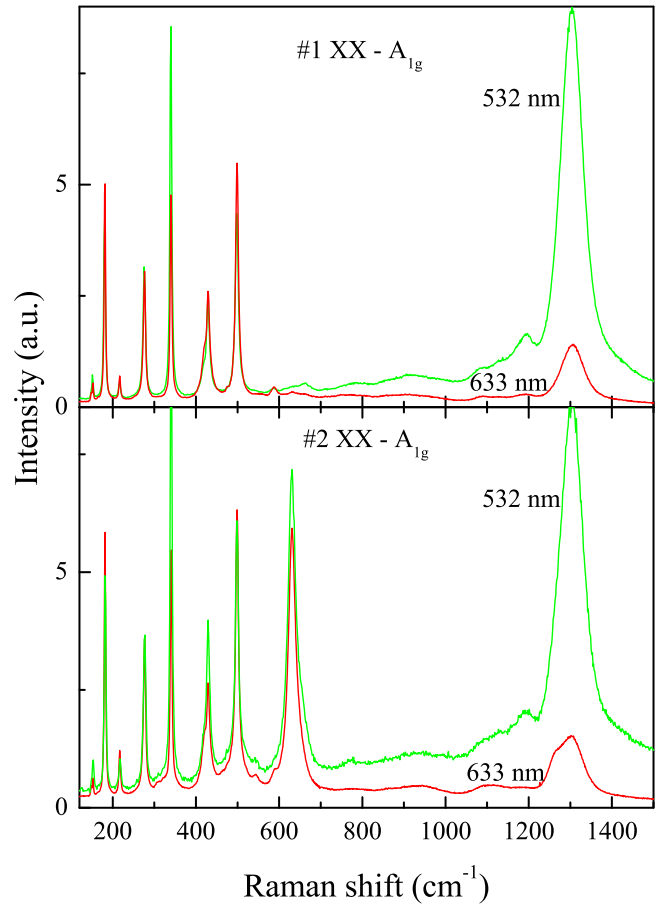


FIG. 9. Raman spectra of two $YFeO_3$ crystals measured with different excitation wavelengths at 300 K.

fluctuations. This mechanism was proposed to explain critical scattering in various antiferromagnets and was used to describe quasielastic scattering in both three-dimensional and low-dimensional materials. It has been shown [38,39] that fluctuations in the total magnetic energy in a magnetic insulator can scatter light, leading to a peak at zero frequency. Its width is determined by the spin-lattice relaxation time, and the integrated intensity is proportional to the magnetic contribution to the heat capacity. Magnetic specific heat in $YFeO_3$ started to increase at $T \geqslant 300$ K as shown in [27]. The mechanism describing such a contribution to the scattering cross section of the quasielasic continuum also determines two-magnon light scattering, i.e., it is associated with scattering by pairs of spin fluctuations. An increase in the intensity of a broad continuum of low-frequency excitations, obviously, may be the reason for asymmetry of a number of phonon lines due to its interaction with phonons.

Therefore, it can be assumed that the additional contribution of spin-phonon effects to the width of phonon lines is the reason for the impossibility of describing the anharmonic contributions by one cubic term in (3) and this scenario should be theoretically analyzed for each mode.

### C. Defect-induced and second-order phonon Raman scattering in $YFeO_3$

In previous Raman studies of $YFeO_3$, not only an extra feature at 630 $cm^{-1}$ was observed, but also another intense line at a doubled frequency near 1300 $cm^{-1}$. Both lines are most intense in polarized geometry ($A_g$ symmetry), but they are also observed with noticeable intensity for $B_{2g}$ symmetry (Figs. 3 and 9, where all intensities are normalized to the intensity of the allowed phonon lines). A change in the excitation energy of the spectra leads to a significant decrease in the intensity of 1300-$cm^{-1}$ line for 633-nm excitation, while the intensity of 630-$cm^{-1}$ line does not change, which clearly indicates the resonance nature of the 1300-$cm^{-1}$ line.

The authors [40] observed the appearance of the 630-$cm^{-1}$ line upon doping of pure $LaFeO_3$ with an admixture of chromium, which is unequivocal evidence of its defective origin. They proposed that the peak at doubled frequency near 1310 $cm^{-1}$ is caused by Frohlich interaction activated two-phonon scattering of the 630-$cm^{-1}$ IR LO mode. Our calculations of the phonon spectrum show that the highest frequencies of IR active vibrations do not exceed 550 $cm^{-1}$, while very flat dispersion curves, including Raman active $B$ modes, are located just in the region of 630 $cm^{-1}$ causing a large peak in the density of phonon states (Fig. 4). We believe that, possibly, as in the case of $LaFeO_3$, the presence

of defects at the site of iron atoms is the reason for the violation of the selection rules for the wave vector and the appearance of phonon excitations with large wave vectors in the Brillouin zone (possibly near the points X, S, and Y) in the observed spectrum. Obviously, the 1300-cm$^{-1}$ peak is caused by second-order scattering, in which phonons with $B$ symmetries with large and oppositely directed wave vectors participate. The selection rules for such scattering in $YFeO_3$ show that the overtones of the $B_{1g}$, $B_{2g}$, and $B_{3g}$ vibrations should be active in $A_g$ symmetry spectra. It is precisely in the polarized geometry of the incident and scattered light that the line at 1300 cm$^{-1}$ is most intense. $B_{2g}$ (XZ) symmetry, in which it is also observed, is allowed for the combination transitions $B_{1g}$*$B_{3g}$.

Often the intensity of defect-induced lines is enhanced by the presence of double resonances because the double-resonance condition can be fulfilled more easily if the sample contains defects which relax the quasimomentum conservation and allow nonzero-phonon wave vectors to contribute to the Raman process. Alternatively, double resonances are observable in two-phonon Raman scattering, where momentum is conserved through phonons of equal but opposite wave vector. The Raman one-phonon and two-phonon scattering spectra in $YFeO_3$ are very similar to spectra in graphite and graphene, where the forbidden phonon with a large wave vector $q$ is also observed in defective samples along with its intense overtone, which is present in a pure sample in the absence of its single-phonon counterpart. The significant intensity of the two-phonon line in graphite is explained by double resonance [41]. This means that energy and momentum conservation are satisfied in all elementary steps of the Raman process. In $YFeO_3$, the peak at 1300 cm$^{-1}$ also has a resonance character, which suggests the important role of double resonance in the appearance of this spectral feature. The appearance of lower-frequency phonons in the two-phonon spectrum (Fig. 9) of defective sample No. 2 for the exciting wavelength of 633 nm may indicate that a different phonon is selected by the double-resonance condition. Of course, a detailed understanding of the possibility of double resonances in $YFeO_3$ requires a more extended study of resonance conditions. The calculation of the electronic spectrum shows the presence of weakly dispersed bands separated by energy gap of about 2–2.5 eV, which can provide such resonance scattering. The band structure obtained from the calculations is shown in Fig. 10. Other much less intense two-phonon features are observed in spectra near 1160–1200 cm$^{-1}$, perhaps they are overtones of the mentioned defect features near 580 cm$^{-1}$.

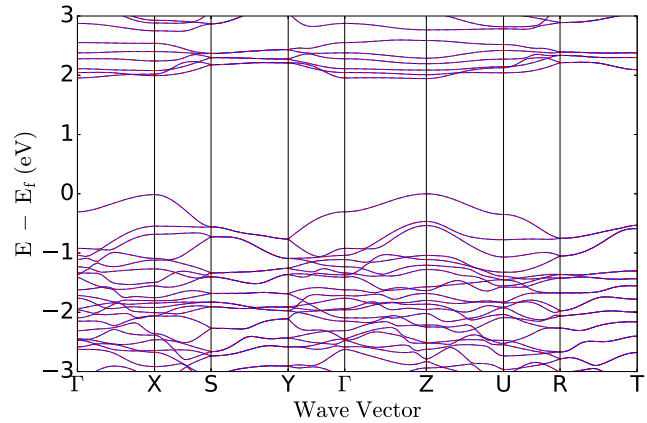


FIG. 10. Calculated electronic band structure of $YFeO_3$. Solid blue and dashed red curves correspond to different spins.

## IV. CONCLUSIONS

Temperature studies of lattice and spin excitations were carried out in $YFeO_3$ single crystal using Raman spectroscopy. The monotonic behavior of phonon frequencies was observed for almost all Raman active phonons without the previously reported sharp anomalies near $T_N$ attributed to spin-phonon effects [5]. A satisfactory fit of the temperature dependencies of the phonon self-energies can be obtained by taking anharmonic contributions into account. However, a number of modes show a more complex temperature behavior, especially for the phonon width. The temperature evolution of the two-magnon peak leads to the appearance of a broad spin-induced continuum in the low-frequency region, which, possibly, determines the renormalization of the phonon self-energies and the observed interference effects. Defect-induced Raman scattering from short-wave phonons, the overtones of which exhibit anomalous intensities in the Raman spectrum due to strong resonance near the excitation energy of about 2.3 eV, has been identified.

## ACKNOWLEDGMENTS

Y.P. is grateful to A. Nosov, who initiated these studies, and also to A. Telegin and S. Naumov for their help in preparing the samples. The research was carried out within the state assignment of the Ministry of Science and Higher Education of the Russian Federation (Grant No. AAAA-A18-118020190098-5, topic "Electron") and was partially supported by the grant of the Russian Foundation for Basic Research (Project No. 19-52-18008).

[1] R. L. White, J. Appl. Phys. **40**, 1061 (1969).
[2] R. M. White, R. J. Nemanich, and C. Herring, Phys. Rev. B **25**, 1822 (1982).
[3] M. Eibschütz, S. Shtrikman, and D. Treves, Phys. Rev. **156**, 562 (1967).
[4] M. Shang, C. Zhang, T. Zhang, L. Yuan, L. Ge, H. Yuan, and S. Feng, Appl. Phys. Lett. **102**, 062903 (2013).
[5] S. Raut, P. D. Babu, R. K. Sharma, R. Pattanayak, and S. Panigrahi, J. Appl. Phys. **123**, 174101 (2018).
[6] G. Lawes, A. P. Ramirez, C. M. Varma, and M. A. Subramanian, Phys. Rev. Lett. **91**, 257208 (2003).
[7] R. M. White, R. J. Nemanich, and C. Tsang, J. Magn. Magn. Mater **15–18**, 773 (1980)
[8] N. Koshizuka and K. Hayashi, J. Phys. Soc. Jpn. **57**, 4418 (1988).

[9] P. V. Coutinho, F. Cunha, and P. Barrozo, Solid State Commun. **252**, 59 (2017).
[10] S. Venugopalan, M. Dutta, A. K. Ramdas, and J. P. Remeika, Phys. Rev. B **31**, 1490 (1985).
[11] M. C. Weber, M. Guennou, H. J. Zhao, J. Íñiguez, R. Vilarinho, A. Almeida, J. A. Moreira, and J. Kreisel, Phys. Rev. B **94**, 214103 (2016).
[12] B. S. Nagrare, S. S. Kekade, B. Thombare, R. V. Reddy, and S. I. Patil, Solid State Commun. **280**, 32 (2018).
[13] H. C. Gupta, M. K. Singh, and L. M. Tiwari, J. Raman Spectrosc. **33**, 67 (2002).
[14] M. K. Singh, H. M. Jang, H. C. Gupta, and R. S. Katiyar, J. Raman Spectrosc. **39**, 842 (2008).
[15] J. Saha and Y. M. Jana, in *2nd International Conference on Condensed Matter and Applied Physics (ICC 2017)*, edited by M. Singh Shekhawat, S. Bhardwaj, and B. Suthar, AIP Conf. Proc. No. 1953 (AIP, New York, 2018).
[16] J.-i. Takahashi, E. Matsubara, T. Arima, and E. Hanamura, Phys. Rev. B **68**, 155102 (2003).
[17] A. P. Kuzmenko, P. V. Abakumov, and M. B. Dobromyslov, J. Magn. Magn. Mater. **324**, 1262 (2012).
[18] A. M. Balbashov, Crystals, **9**, 487 (2019).
[19] P. E. Blöchl, Phys. Rev. B **50**, 17953 (1994).
[20] G. Kresse and J. Furthmuller, Phys. Rev. B **54**, 11169 (1996).
[21] J. P. Perdew, K. Burke, and M. Ernzerhof, Phys. Rev. Lett. **77**, 3865 (1996).
[22] V. I. Anisimov, F. Aryasetiawan, and A. I. Lichtenstein, J. Phys.: Condens. Matter **9**, 767 (1997).
[23] D. Stoeffler and Z. J. Chaker, Magn. Magn. Mater. **442**, 255 (2017).
[24] A. Togo and I. Tanaka, Scr. Mater. **108**, 1 (2015).
[25] P. G. Klemens, Phys. Rev. **148**, 845 (1966).
[26] M. Balkanski, R. F. Wallis, and E. Haro, Phys. Rev. B **28**, 1928 (1983).
[27] H. Shena, J. Xua, A. Wua, J. Zhaoa, and M. Shia, Mater. Sci. Eng. B **157**, 77 (2009).
[28] Y. Su, J. Guo, X. Cheng, S. Feng, and Y. Yang, J. Alloys Compd. **805**, 489 (2019).
[29] A. K. Mall, B. Paul, A. Garg, and R. Gupta, J. Raman Spectrosc. **51**, 537 (2020).
[30] T. Shen, Y. Feng, C. Hu, H. Dai, M. Song, W. Yang, H. Liu, and X. Wei, Optoelectron. Adv. Mater. Rapid Commun. **10**, 268 (2016).
[31] M. V. Klein, in *Light Scattering in Solids*, edited by M. Cardona (Springer, Berlin, 1975), p. 174.
[32] S. M. Shapiro, J. D. Axe, and J. P. Remeika, Phys. Rev. B **10**, 2014 (1974).
[33] S. E. Hahn, A. A. Podlesnyak, G. Ehlers, G. E. Granroth, R. S. Fishman, A. I. Kolesnikov, E. Pomjakushina, and K. Conder, Phys. Rev. B **89**, 014420 (2014).
[34] P. Knoll, C. Thomsen, M. Cardona, and P. Murugaraj, Phys. Rev. B **42**, 4842 (1990).
[35] Y. S. Ponosov, G. A. Bolotin, and N. M. Chebotaev, Phys. Lett. A **146**, 551 (1990).
[36] T. M. H. Nguyen, L. J. Sandilands, C. H. Sohn, C. H. Kim, A. L. Wysocki, I.-S. Yang, S. J. Moon, J.-H. Ko, J. Yamaura, Z. Hiroi, and T. W. Noh, Nat. Commun. **8**, 251 (2017).
[37] P. Lemmens, G. Guntherodt, and C. Gros, Phys. Rep. **375**, 1 (2003).
[38] G. F. Reiter, Phys. Rev. B **13**, 169 (1976).
[39] J. W. Halley, Phys. Rev. Lett. **41**, 1605 (1978).
[40] J. Andreasson, J. Holmlund, R. Rauer, M. Käll, L. Börjesson, C. S. Knee, A. K. Eriksson, S.-G. Eriksson, M. Rübhausen, and R. P. Chaudhury, Phys. Rev. B **78**, 235103 (2008).
[41] D. M. Basko, S. Piscanec, and A. C. Ferrari, Phys. Rev. B **80**, 165413 (2009).